Oil Shale, 2023, Vol. 40, No. 4, pp. 321–343
doi: https://doi.org/10.3176/oil.2023.4.03
ISSN 0208-189X

Study on the pyrolysis behavior and kinetics of Jimusar oil shale with H_2O/CO_2 injection

Dongwei Huang[a,b], Zhiqin Kang[a,b], Dong Yang[a,b], Ran Cao[a,b], Zhenni Cui[c], Yang Lu[a,b]*

(a) Key Laboratory of In-Situ Property-Improving Mining of Ministry of Education, Taiyuan University of Technology, Taiyuan 030024, China
(b) The In-Situ Steam Injection Branch of State Center for Research and Development of Oil Shale Exploitation, Taiyuan University of Technology, Taiyuan 030024, China
(c) State Key Laboratory of Clean and Efficient Coal Utilization, Taiyuan University of Technology, Taiyuan 030024, China

Received 13 April 2023, accepted 13 October 2023, available online 10 November 2023

Abstract. *High-temperature water vapor (H_2O) and carbon dioxide (CO_2) improved the yield and quality of shale oil during oil shale pyrolysis. Aiming to fill knowledge gaps regarding the kinetic mechanism of oil shale pyrolysis in different atmospheres, the pyrolysis behavior and kinetics of Jimusar (JM) oil shale with H_2O, CO_2 and N_2 injections were fully studied in this paper. The results revealed that compared with the N_2 injection, the presence of both H_2O and CO_2 increased the mass loss and mass loss rate, advanced the initial precipitation temperature as well as peak temperature and moved the pyrolysis zone to the low-temperature zone, indicating that both H_2O and CO_2 injections promoted the pyrolysis behavior of oil shale. The comprehensive release characteristic index of volatiles during oil shale pyrolysis at the heating rate of 20 °C/min with H_2O and CO_2 injections increased by 37.02% and 18.94%, respectively, which significantly improved pyrolysis reactivity; so, the effect of the H_2O injection was higher than that of the CO_2 injection. The average activation energy of Jimusar oil shale pyrolysis was as follows: the first stage < the second stage < the third stage. During oil shale kerogen pyrolysis (the second stage), the activation energies with N_2, CO_2 and H_2O injections exhibited an initial rising trend, then a decreasing trend followed by a constantly decreasing trend and a fluctuating trend with an increase in the conversion rate, respectively. The presence of H_2O and CO_2 changed the pyrolysis mechanism of oil shale kerogen from a first-order model to a diffusion model. The kinetic mechanism functions of oil shale pyrolysis with N_2, CO_2 and H_2O injections were $f(\alpha) = 1-\alpha$, $f(\alpha) = [-\ln(1-\alpha)]^{-1}$, and $f(\alpha) = 1.5(1-\alpha)^{2/3}[1-(1-\alpha)^{1/3}]^{-1}$, respectively. The pyrolysis conversion curves of Jimusar oil shale with N_2, CO_2 and H_2O injections obtained from the kinetic parameters were consistent with the experimental curves.*

* Corresponding author: e-mail *luyang0116@link.tyut.edu.cn*

Keywords: *Jimusar oil shale, pyrolysis, water vapor, CO_2, kinetics.*

1. Introduction

China is rich in oil shale resources, ranking second worldwide, with the majority of resources located in Huadian, Jilin, Maoming, Guangdong, Fushun, Liaoning, and Jimusar, Xinjiang [1]. Oil shales are greyish-brown or black in color with a dense lamellar structure and copious amounts of organic kerogen [2]. Kerogen is a complex macromolecule with a three-dimensional network structure. Its molecular structure is dominated by aliphatic hydrocarbons with a few aromatic structures and a small number of oxygen-containing groups, which are the main sources of pyrolytic hydrocarbons. Oil shale is a hydrogen-rich fuel with high hydrogen/carbon (H/C) ratio; the properties of the oil shale generated through pyrolysis are similar to those of "natural oil". Therefore, oil shale is a highly important strategic reserve and supplementary energy source for China [3]. However, due to the high ash content and poor heat transfer efficiency of oil shale, the pyrolysis oil yield is low and the oil product quality is poor. Therefore, improving the oil shale pyrolysis efficiency and quality is essential.

Notably, the atmosphere is a factor that affects the pyrolysis behavior and kinetics of oil shale and participates in chemical reactions during pyrolysis. The introduction of water vapor (H_2O) and carbon dioxide (CO_2) into the oil shale pyrolysis system effectively increases pyrolysis efficiency and improves the quality of the pyrolysis oil products [4]. Scholars have conducted research on the pyrolysis behavior and kinetics of oil shale under different atmospheric conditions. Bai et al. [5] studied the influence of the CO_2 concentration on the thermal decomposition behavior of oil shale and found that the addition of CO_2 first increased the total weight loss of oil shale and then decreased, indicating that a small amount of CO_2 assisted in oil shale pyrolysis. Kang et al. [6] studied the impact of H_2O and CO_2 injections on oil quality during pyrolysis. The results showed that both H_2O and CO_2 improved the quality of oil shale pyrolysis and increased the content of light components, with the effect of H_2O being superior to that of CO_2. However, pertinent kinetic studies are lacking. Wang et al. [7] studied the reaction mechanism of Fushun oil shale and kerogen pyrolysis under inert atmospheric conditions and calculated their average activation energies using the Flynn-Wall-Ozawa (FWO) and Friedman kinetic methods. The activation energies of the resulting oil shale pyrolysis were 237.63 kJ/mol and 236.80 kJ/mol, respectively. Ma et al. [8] established a two-stage kinetic model using asphalt as an intermediate product. The results showed that the apparent activation energy of hot asphalt generated by kerogen pyrolysis (110 kJ/mol) was lower than that of the oil shale further decomposed by hot asphalt (190 kJ/mol). Furthermore, it was also discovered that the pyrolysis temperature of oil shale in a saturated water medium was

about 120 °C lower than that under anhydrous conditions. Liang et al. [9] studied the activation energy of Huadian oil shale in different pyrolysis stages using the first-order reaction model and Doyle integral method, and found that the activation energy in the second oil shale pyrolysis stage was higher than that in the first and third stages. The second stage is the main stage of organic matter decomposition in oil shale and requires a high amount of energy to break the chemical bonds in the organic matter. Zhao et al. [10] conducted pyrolysis experiments on oil shale under non-isothermal conditions with N_2 and CO_2 as thermal-carrying fluids and confirmed that compared with N_2, CO_2 reduced the activation energy of oil shale because it redounds the liberation of volatile matter during the second stage of oil shale pyrolysis.

In summary, previous studies demonstrated the effect of the CO_2 or H_2O injection on oil shale pyrolysis product quality and calculated the corresponding average activation energy under inert atmospheres. However, there have been limited reports on the kinetic mechanisms and models of oil shale pyrolysis at different stages with CO_2 and H_2O injections. Therefore, by studying the thermal decomposition behavior of oil shale with the N_2, CO_2, or H_2O injection at different heating rates, we assessed the pyrolysis kinetic parameters and explored the effects of different atmospheres on the oil shale pyrolysis mechanism to provide a theoretical basis for the clean and efficient utilization of oil shale.

2. Experimental materials and methods

2.1. Oil shale sample

The sample was obtained from Jimusar, Xinjiang, China, and is herein referred to as Jimusar (JM) oil shale. Prior to the experiment, the oil shale was crushed into powder with a diameter of ≤ 0.15 mm, which was then dried and dehydrated for 24 h at 105 °C and sealed for reserve. The results of proximate analysis and ultimate analysis (GB/T 212-2008 and GB/T 476-2008) for JM oil shale are presented in Table 1. As shown in Table 1, the volatile content (*V*) of JM oil shale was high, accounting for 43.86 ω_{ad} %, and the water (*M*) and fixed carbon (*FC*) contents were low. The atomic ratios H/C and O/C were 1.53 and 0.09, respectively. According to the van Krevelen diagram, kerogen is Type I and has good oil-generating potential [11].

Table 1. Proximate analysis and ultimate analysis of Jimusar oil shale

Sample	Proximate analysis, ω_{ad} %				Ultimate analysis, ω_{ad} %				
	M	A	V	FC	C	H	O	N	S_t
JM	0.15	52.05	43.86	3.94	39.31	5.02	4.69	1.39	0.79

Note: ad means on air dried basis

2.2. Thermogravimetric experiment

An STA449F3 synchronous thermal analyzer was used for the experiment, and the temperature error was ±1 °C. The mass of the sample used in thermogravimetric (TG) experiments was 30.0 ± 0.1 mg. The experimental temperature was increased from room temperature to 900 °C at heating rates of 10, 20, and 30 °C/min. The pyrolysis atmosphere was injected with N_2, CO_2, or H_2O at a flow rate of 70 mL/min. The effect of each injection (N_2, CO_2, and H_2O) was investigated at all three heating rates. TG and differential TG (DTG) data for oil shale pyrolysis were obtained and each experiment was repeated at least three times.

2.3. Pyrolysis parameters

To further evaluate the pyrolysis behavior of JM oil shale, we introduced the following pyrolysis characteristic parameters.

2.3.1. The initial precipitation temperature of volatiles

The initial precipitation temperature of the volatile (*Tv*) was the main indicator for evaluating the oil shale pyrolysis characteristics. The lower the *Tv* value, the better the oil shale pyrolysis performance [12]. Generally, the temperature corresponding to the lowest weight loss rate in the drying and degassing stages of oil shale pyrolysis is defined as *Tv*.

2.3.2. Half-peak width

The half-peak width is the temperature range when $(dw/dt)/(dw/dt)_{max}$ (%/min) is 0.5, where $(dw/dt)_{min}$ and $(dw/dt)_{max}$ are the minimum and maximum weight loss rates (%/min) on the DTG curve, respectively. It was used to evaluate the concentration degree of oil shale volatile discharge during pyrolysis.

2.3.3. The comprehensive release characteristic index of volatiles

The comprehensive release characteristic index of volatiles (*D*) is a major index for evaluating oil shale pyrolysis reactivity [13]. The higher the *D* value, the faster the reaction of oil shale, and the higher the volatile release rate. As a result, the pyrolysis reactivity was improved. *D* was calculated using Eq. (1):

$$D = \frac{\left(dw/dt\right)_{max} \times \left(dw/dt\right)_{mean}}{T_V \times T_{max} \times \Delta T_{1/2}}, \tag{1}$$

where $(dw/dt)_{mean}$ (%/min) is the average weight loss rate and T_{max} (°C) is the peak temperature corresponding to the maximum weight loss rate.

2.4. Kinetic analysis

The apparent activation energy of JM oil shale pyrolysis was obtained using the isoconversional method. A, E, and $f(\alpha)$ are the kinetic triplet, $A(s^{-1})$ is the pre-exponential or frequency factor, E (kJ/mol or kcal/mol) is the activation energy, and $f(\alpha)$ is a function which depends on the reaction mechanism. For pyrolysis under non-isothermal conditions, the constant heating rate $\beta = dT/dt$, and the corresponding kinetic equation is expressed by Eq. (2) [14]:

$$\frac{d\alpha}{dt} = \frac{A}{\beta} \cdot \exp\left(-\frac{E}{RT}\right) \cdot f(\alpha), \tag{2}$$

where R is the universal gas constant of 8.3145 J·(mol·°C)$^{-1}$; T (°C) is the temperature; and α is the conversion degree. $\alpha = (m_p - m_t)/(m_p - m_{p+1})$ (p = 1, 2, 3), in which m_p, m_t, and m_{p+1} are the initial mass at stage p, mass at pyrolysis time t, and mass at the end of pyrolysis at the same stage, respectively.

Integral methods such as the FWO and Kissinger-Akahira-Sunose (KAS) methods were used to calculate the activation energy. The expressions for the two dynamic equations are as follows (Eqs. (3–4)):

FWO method:

$$\ln\beta = \ln\left(\frac{AE}{RG(\alpha)}\right) - 5.331 - 1.0516\frac{E}{RT}, \tag{3}$$

KAS method:

$$\ln\left(\frac{\beta}{T^2}\right) = \ln\left(\frac{AE}{RG(\alpha)}\right) - \frac{E}{RT}, \tag{4}$$

where $G(a)$ is the mechanism function in the integral form. The 15 most frequently used solid-phase reaction dynamic mechanism functions [15] are listed in Table 2. The relationship between $G(\alpha)$ and $f(\alpha)$ is expressed by Eq. (5):

$$G(\alpha) = \int_0^\alpha \frac{1}{f(\alpha)} d\alpha . \tag{5}$$

We took the reaction temperature T corresponding to the reaction conversion α of 0.2, 0.3, 0.4, 0.5, 0.6, 0.7, and 0.8 at β of 10, 20, and 30 °C/min, respectively. At the same conversion rate, three data points corresponding to the heating rate β and temperature T were obtained and were denoted as groups. 1/T was plotted using $\ln(\beta)$ (FWO method) and $\ln(\beta/T^2)$ (KAS method). The least-squares method was used for the linear regression of each data group, and the slope k was obtained to determine the activation energy at the corresponding conversion rate. The activation energy was –kR/1.0516 using the FWO and –kR using the KAS method, respectively.

Table 2. The most frequently used mechanisms of solid state process

Reaction mechanism	Symbol	$f(\alpha)$	$G(\alpha)$
Order of reaction			
First-order	F_1	$1-\alpha$	$-\ln(1-\alpha)$
Second-order	F_2	$(1-\alpha)^2$	$(1-\alpha)^{-1}-1$
Third-order	F_3	$(1-\alpha)^3$	$[(1-\alpha)^{-2}-1]/2$
Diffusion			
One-way transport	D_1	$0.5\alpha^{-1}$	α^2
Two-way transport	D_2	$[-\ln(1-\alpha)]^{-1}$	$(1-\alpha)\ln(1-\alpha)+\alpha$
Three-way transport	D_3	$1.5(1-\alpha)^{2/3}[1-(1-\alpha)^{1/3}]^{-1}$	$[1-(1-\alpha)^{1/3}]^2$
Ginstling-Brounshtein equation	D_4	$1.5[(1-\alpha)^{-1/3}-1]^{-1}$	$(1-2\alpha/3)-(1-\alpha)^{2/3}$
Limiting surface reaction between both phases			
One dimension	R_1	1	α
Two dimensions	R_2	$2(1-\alpha)^{1/2}$	$1-(1-\alpha)^{1/2}$
Three dimensions	R_3	$3(1-\alpha)^{2/3}$	$1-(1-\alpha)^{1/3}$
Random nucleation and nuclei growth			
Two-dimensional	A_2	$2(1-\alpha)[-\ln(1-\alpha)]^{1/2}$	$[-\ln(1-\alpha)]^{1/2}$
Three-dimensional	A_3	$3(1-\alpha)[-\ln(1-\alpha)]^{2/3}$	$[-\ln(1-\alpha)]^{1/3}$
Exponential nucleation			
Power law, n = 1/2	P_2	$2\alpha^{1/2}$	$\alpha^{1/2}$
Power law, n = 1/3	P_3	$3\alpha^{2/3}$	$\alpha^{1/3}$
Power law, n = 1/4	P_4	$4\alpha^{3/4}$	$\alpha^{1/4}$

3. Results and discussion

3.1. Pyrolysis behavior of oil shale

Figure 1 shows the TG and DTG curves of JM oil shale injected with N_2, CO_2, and H_2O and heated from room temperature to 900 °C (β = 30 °C/min). From the TG curves it can be observed that with increasing temperature, the oil shale organic matter gradually cracked and that CO_2 and H_2O increased its

weight loss, which promoted the cracking process and released the volatile fraction. The order of maximum weight loss under the three atmospheres was $H_2O > CO_2 > N_2$. The DTG curves show that the oil shale pyrolysis under all three atmospheres exhibited a notable peak weight loss from 350 °C to 550 °C. In this temperature range, unstable chemical bonds break to produce a large amount of free radicals, which combine to form and release volatile hydrocarbons, and abundant polycyclic aromatic hydrocarbons polymerize to form shale coke. From 550 °C to 900 °C, the organic matter of oil shale pyrolyzed to completion without a notable change in weight loss. The N_2 injection led to the second weight loss peak at a temperature ranging from 700 to 800 °C, which was likely due to the decomposition of carbonates. However, CO_2 and H_2O injections did not lead to the second weight loss peak, indicating that both CO_2 and H_2O could inhibit the decomposition of carbonates, which was consistent with the conclusions of previous studies [5, 6]. Compared with the N_2 injection, the increased pyrolysis weight loss rate of oil shale injected with CO_2 and H_2O indicated that these compounds were involved in the reaction of organic matter, promoted its cleavage and released the volatile fraction from oil shale [16–18]. Figure 1 reveals that CO_2 and H_2O injections moved the oil shale pyrolysis process toward the low-temperature zone, enabling pyrolysis at lower temperatures. This likely resulted from the fact that during oil shale pyrolysis, CO_2 reacted with methane (CH_4) catalyzed by intrinsic minerals ($CO_2 + CH_4 = 2CO + 2H_2$), and H_2O reacted with CO gas catalyzed by intrinsic minerals ($CO + H_2O = CO_2 + H_2$) [19–21]. Notably, the H_2O injection was more effective than that of CO_2.

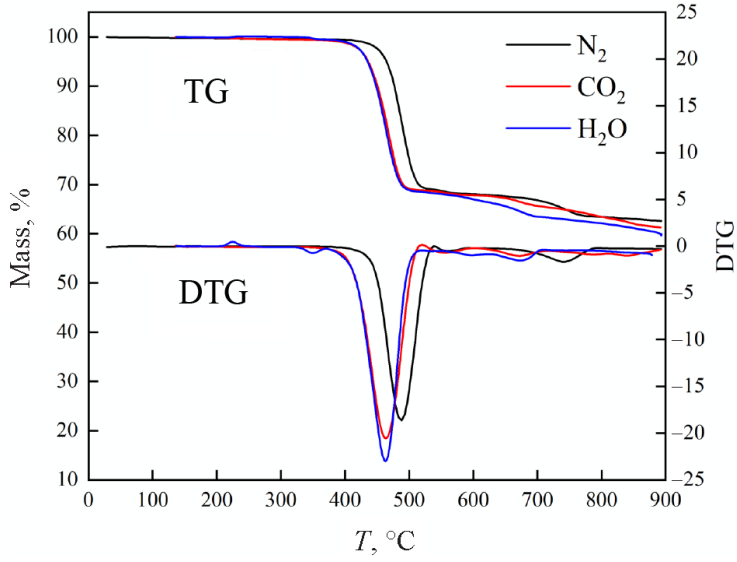

Fig. 1. TG and DTG curves of oil shale in different atmospheres (β = 30 °C/min).

3.2. Pyrolysis characteristic parameters of oil shale in different atmospheres

The pyrolysis characteristics and errors of oil shale at different heating rates under the three atmospheres are listed in Table 3. The results showed that T_v and T_{max} of oil shale pyrolysis after CO_2 and H_2O injections were lower than after the N_2 injection, indicating that the former two injections allowed the oil shale pyrolysis reaction to proceed at lower temperatures. With CO_2 and H_2O injections, T_v was reduced by 25.4–35.1 °C and 23.6–35.5 °C, respectively, and T_{max} was decreased by 20.6–30.4 °C and 17.1–28.2 °C, respectively, while D increased by 9.59–18.94% and 26.91–37.02%, respectively, compared with the N_2 injection. Both CO_2 and H_2O injections slightly increased the half-peak width ($\Delta T_{1/2}$). These results demonstrated that the introduction of CO_2 and H_2O, to some extent, promoted the precipitation of small-molecule gases and the formation of well-developed pore structures, which was conducive to oil shale mass and heat transfer during pyrolysis [22]. Thus, both CO_2 and H_2O injections advanced the release of volatiles and effectively improved the pyrolytic reactivity of oil shale, with the H_2O injection being more effective than that of CO_2.

As shown in Table 3, with increasing β, T_v decreased, but T_{max}, $(dw/dt)_{max}$ (%/min), $(dw/dt)_{mean}$ (%/min), and $\Delta T_{1/2}$ were cumulative by degrees. The D value of oil shale clearly increased in all three atmospheres. With CO_2 and H_2O injections at β = 30 °C/min the D was 6–7 times higher than that at β = 10 °C/min. The accretion of the heating rate enhanced the heat difference and pressure gradient inside and outside the oil shale and boosted its resistance to mass and heat transfers, which caused thermal hysteresis [23]. Additionally, an increase in the heating rate led to a swift increase in the internal temperature of oil shale and heat supply, which resulted in a violent oil shale pyrolysis reaction and an early release of volatile oil and gas. This also increased the weight loss rate of the entire pyrolysis process. Therefore, increasing β could substantially magnify the pyrolysis characteristics of oil shale [24, 25].

3.3. Analysis of kinetic parameters

3.3.1. Calculation of activation energy

Figure 2 shows the activation energies of JM oil shale at different conversion rates during each pyrolysis stage under three different pyrolysis atmospheres, N_2, CO_2, and H_2O, calculated using the FWO and KAS methods. The differences between the activation energies calculated using the two methods were insignificant, confirming the accuracy of the calculation results. As shown in Figure 2a, the activation energy of JM oil shale pyrolysis in the first pyrolysis stage increased gradually with increasing temperature under the three atmospheres. At a conversion rate of 0.2–0.6, the temperature increased from room temperature to 200 °C at which water and small gas molecules

Table 3. Pyrolysis characteristics of Jimusar oil shale in N_2, CO_2 and H_2O atmospheres

Atmosphere	Heating rate, °C min^{-1}	T_v, °C	T_{max}, °C	$(dw/dt)_{max}$, °C min^{-1}(error)	$(dw/dt)_{mean}$, °C min^{-1}(error)	$\Delta T_{1/2}$, °C(error)	$D \times 10^{-7}$, %^{2} min^{-2} °C^{-3}(error)
N_2	10	433.4	473.5	7.72(8.11%)	0.44(6.20%)	35.3(3.52%)	4.69(6.66%)
	20	432.6	488.6	14.03(8.48%)	0.86(7.84%)	38.0(5.27%)	14.99(6.29%)
	30	430.0	488.3	21.10(9.66%)	1.31(9.31%)	38.8(6.95%)	33.93(5.11%)
CO_2	10	408.0	444.8	7.14(7.64%)	0.53(8.51%)	40.6(7.90%)	5.14(7.61%)
	20	401.0	458.2	14.84(8.04%)	0.98(7.12%)	44.4(6.44%)	17.83(8.19%)
	30	394.9	467.7	22.55(8.35%)	1.57(7.63%)	47.8(8.78%)	40.10(10.16%)
H_2O	10	409.8	456.4	7.84(10.10%)	0.54(9.26%)	35.6(6.82%)	6.34(8.69%)
	20	401.7	460.4	15.23(10.38%)	1.07(10.67%)	42.9(8.75%)	20.54(9.58%)
	30	394.5	463.4	22.98(11.12%)	1.61(10.98%)	47.0(7.44%)	43.06(9.77%)

were thermally removed and organic matter with lower bond energy was gradually pyrolyzed with low activation energy. Subsequently, at a conversion rate of 0.6–0.8, the temperature increased from 200 °C to 350 °C, conducive to the conversion of kerogen into asphaltene, which requires a higher amount of energy [26].

(a)

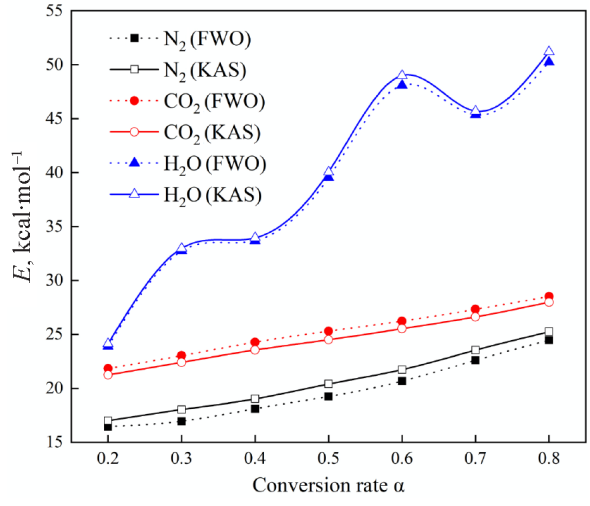

(b)

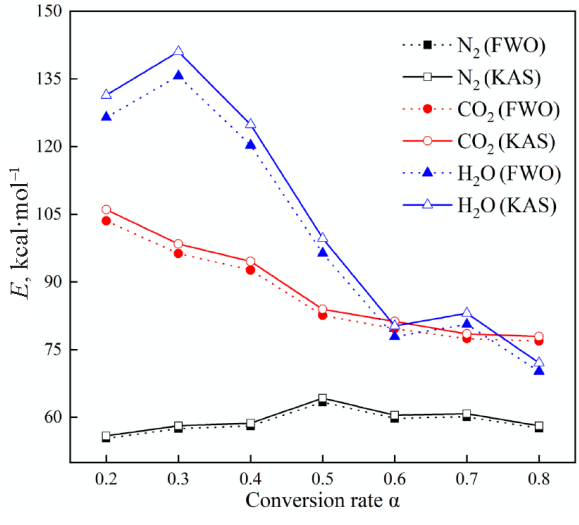

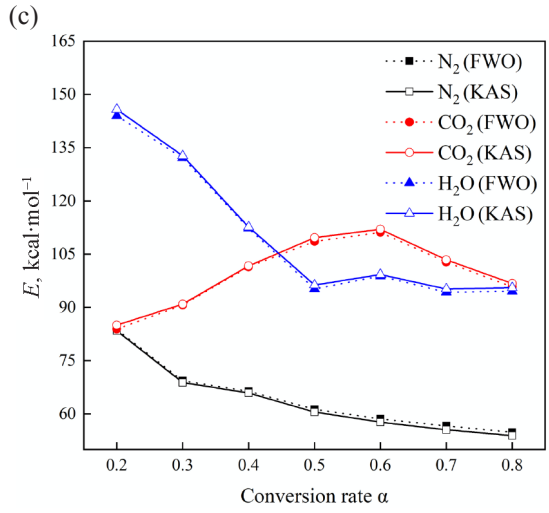

Fig. 2. Apparent activation energy of Jimusar oil shale in three atmospheres at different conversion rates and pyrolysis stages: (a) stage I at 350 °C, (b) stage II at 350–550 °C, (c) stage III at 500–900 °C.

As shown in Figure 2b, during the second pyrolysis stage, the activation energy of JM oil shale in the three atmospheres showed different trends at different conversion rates. An increase in conversion rate with the N_2 injection led to a gradual increase in temperature, while the activation energy first increased and then decreased, reaching a maximum value of 64.5 kcal/mol at a conversion rate of 0.5 and a reaction temperature of around 470.5–486.0 °C. The maximum pyrolysis rate of JM oil shale was reached, and a large number of chemical bonds in the organic matter broke to form free radicals (such as R_2R_3" = $R_2\cdot$ + $R_3\cdot$ or R_1H" = $R_1\cdot$ + H·), so that the activation energy reached a maximum [19].

The activation energy gradually decreased from 105.1 kcal/mol to 76.4 kcal/mol after the CO_2 injection, but fluctuated with the H_2O injection, reaching a maximum of 140 kcal mol^{-1} at a conversion rate of 0.3 and a minimum of 71 kcal mol^{-1} at a conversion rate of 0.8. There was an insignificant difference in activation energy between oil shale pyrolyses with CO_2 and H_2O injections at a conversion rate of 0.6–0.8. This was observed at 400–450 °C at the second pyrolysis stage with CO_2 and H_2O injections at a conversion rate of 0.2–0.3, while the activation energy of the second stage was the highest. This is because at 350–450 °C, a substantial quantity of organic matter in oil shale started to pyrolyze, requiring a large amount of energy, and, as just shown in Table 3, T_v with CO_2 and H_2O injections was around 400 °C. Additionally, water acted as an efficient acid or base catalyst or as an acid-base double catalyst. These catalytic effects could be enhanced by the presence of intrinsic minerals in oil shale, such as dolomite, and the generation of certain products during the reaction acts as a pyrolysis auto catalyst [19].

As shown in Figure 2c, during the third stage of pyrolysis, the activation energy resulting from N_2 and H_2O injections gradually decreased because the pyrolysis reaction of organic matter in oil shale was completed and the pyrolysis products were gradually discharged. The high temperature water vapor from the H_2O injection inhibited the decomposition of carbonate, which further reduced the activation energy. Thus, the activation energy resulting from the CO_2 injection first increased and then decreased, reaching a maximum value at a conversion rate of 0.6 and a temperature of 775–783 °C. This could be attributed to the gasification of excess CO_2 with C at high temperatures ($CO_2 + C = 2\ CO$), the secondary hydrocarbon reaction of the hydrocarbon pyrolysis products with CO_2 ($C_mH_n + CO_2 = 2m\ CO + n/2\ H_2$), and the water-gas conversion reaction ($CO + H_2O = CO_2 + H_2$) [27, 28]. The activation energy during the third pyrolysis stage tended to increase and then decrease slightly due to the inhibition of carbonate decomposition by CO_2, CO_2 and H_2O also inhibited the secondary polymerization of small molecules at high temperatures, resulting in low activation energies [29]. Figure 2c displays that at a conversion rate of 0.2–0.4 the activation energy of oil shale pyrolysis in the H_2O atmosphere was higher than in the CO_2 atmosphere, while the opposite was true at a conversion rate of 0.5–0.8. A possible reason for this could be attributed to the high energy requirement during the reaction of excess CO_2 with C and the reaction of the hydrocarbon pyrolysis products.

Figure 3 exhibits the average activation energies of each pyrolysis stage calculated using the FWO and KAS methods. The correlation coefficient R^2 was > 0.98, indicating a high linear correlation. As shown in Figure 3, the average activation energy of JM oil shale during pyrolysis was ranked

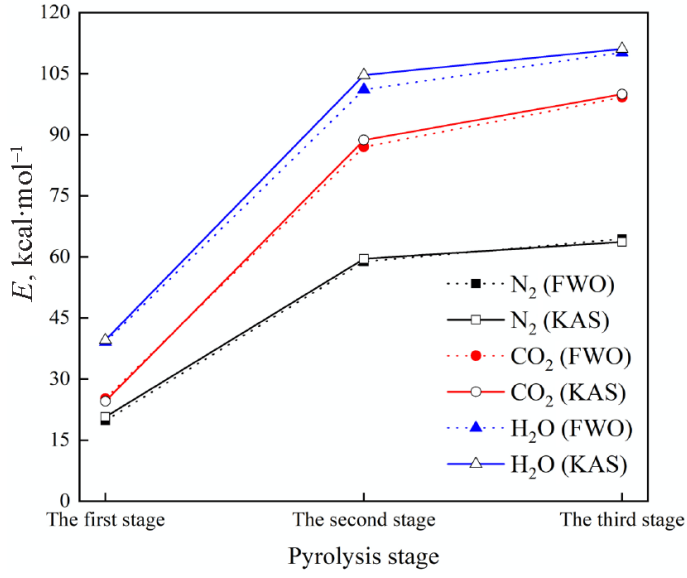

Fig. 3. Average apparent activation energy at each pyrolysis stage in three atmospheres.

as follows: the first stage < the second stage < the third stage. During the first stage of JM oil shale pyrolysis, the temperature was below 350 °C, the water and organic light components inside oil shale were thermally removed, some low bond energy chemical bonds decomposed, the organic matter was converted into bitumen, and the average activation energy at this stage was the lowest. With an increase in temperature, the reaction continued and most organic matter started to be fully decomposed by heat during the second stage of oil shale pyrolysis. This process required a large amount of energy and the activation energy higher than that of pyrolysis of kerogen into bitumen. During the third stage, the activation energy increased slightly, mainly because of the decomposition of organic matter and minerals with high chemical bonding energies [9]. The activation energy of oil shale pyrolysis during this stage was the highest among the three stages.

The average activation energy for each JM oil shale pyrolysis stage in the three atmospheres was ranked as $N_2 < CO_2 < H_2O$ for three reasons [30]. First, the specific heat capacity of N_2 was the smallest and that of H_2O was the highest; and, the higher the specific heat capacity, the higher the energy requirement to increase at the same temperature. Second, CO_2 promoted the breaking of O–H and C–H bonds and the thermal cracking of pyrolytic volatiles [31]. H_2O produced free radicals (such as H• and OH•) under the catalytic effects of CO gas and intrinsic minerals in the atmosphere. This facilitated kerogen pyrolysis in CO_2 and H_2O atmospheres, which required more energy and increased the weight loss rate of oil shale pyrolysis occurring during the second pyrolysis stage. Third, both CO_2 and H_2O increased the activation energy through secondary reactions with the volatile fraction, which mainly happened during the third stage.

3.3.2. Calculation of mechanism function and pre-exponential factor A

The shapes of the experimental and standard curves were compared to determine the most probable pyrolysis reaction mechanism function. The principal curve method is more intuitive and reliable than the traditional numerical method for determining mechanism functions. In this study, the integral principal curve method was used for the above purpose.

The dynamic equation in integral form is shown in Eq. (6):

$$\begin{aligned} G(\alpha) &= \int_0^{\alpha} \frac{1}{f(\alpha)} \mathrm{d}\alpha = \frac{A}{\beta} \int_{T_0}^{T} \exp\left(-\frac{E}{RT}\right) \mathrm{d}T, \\ &\approx \frac{A}{\beta} \int_0^{T} \exp\left(-\frac{E}{RT}\right) \mathrm{d}T = \frac{AE}{\beta R} P(u), \end{aligned} \tag{6}$$

where T_0 is the initial temperature of the reaction, and $u = E/RT$. The Doyle approximation was used to solve the temperature integral, as shown in Eq. (7) [32]:

$$P(u) = 0.00484 \cdot \exp(-1.051\text{-}6u), \tag{7}$$

where $P(u)$ is the temperature integral. Eqs. (8)–(9) can be obtained by selecting a conversion rate (α) of 0.5:

$$G(0.5) = \frac{AE}{\beta R} P(u_{0.5}), \tag{8}$$

$$\frac{G(\alpha)}{G(0.5)} = \frac{P(u)}{P(u_{0.5})}, \tag{9}$$

where $P(u_{0.5})$ is the temperature integral at a conversion rate (α) of 0.5.

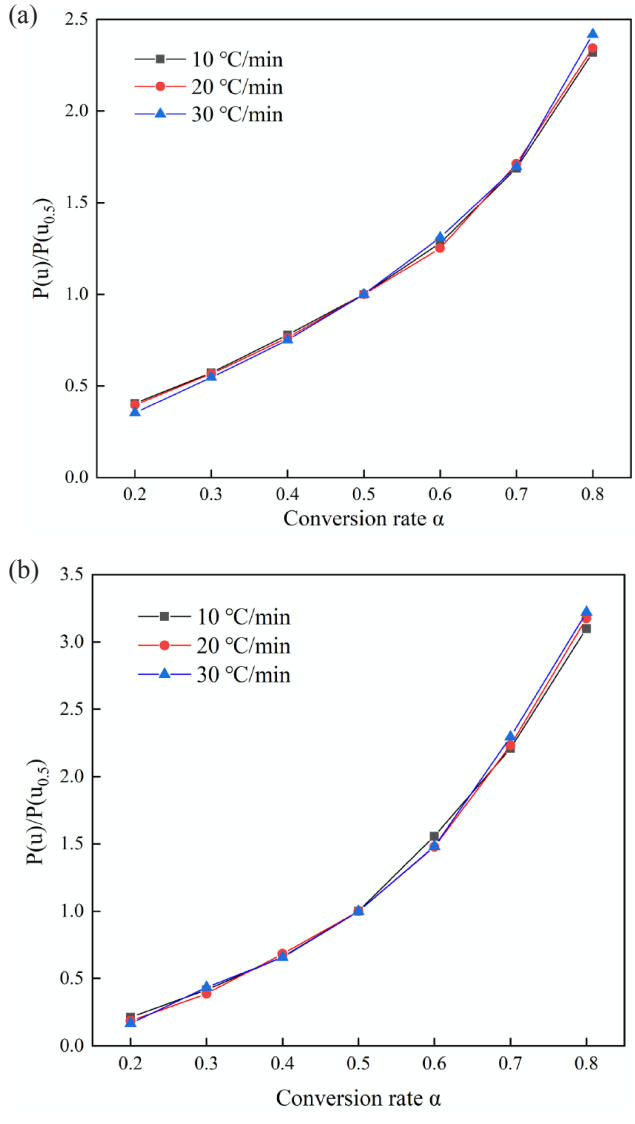

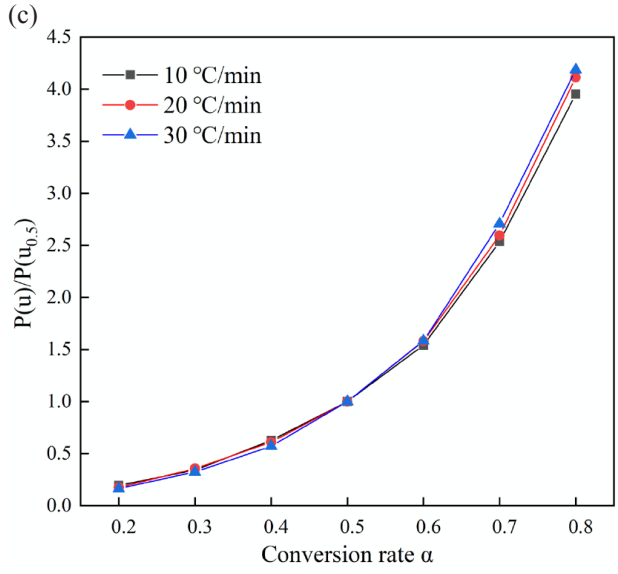

Fig. 4. Experimental curves of the second stage of Jimusar oil shale pyrolysis at different heating rates in three atmospheres: (a) N_2, (b) CO_2, (c) H_2O.

For the 15 common kinetic model functions (Table 2), a series of standard curves were obtained by plotting $G(a)/G(0.5)$ against α in the three atmospheres. To better understand the reaction mechanism of organic matter during JM oil shale pyrolysis, the average activation energy E in the second pyrolysis stage and the corresponding temperatures of the three heating rates at different conversion rates were selected and substituted into Eq. (7) to derive $P(u)/P(u_{0.5})$. Three experimental curves were obtained at different heating rates, as shown in Figure 4. The experimental curves corresponding to different heating rates in the three atmospheres were in accordance with each other, indicating that the JM oil shale pyrolysis mechanism in the second stage was unaffected by heating rate and could be described by the same dynamic mechanism function. The experimental curves of JM oil shale during the second pyrolysis stage were compared with the standard curves in the three atmospheres with β = 20 °C/min, as shown in Figure 5. The experimental curves for N_2, CO_2, and H_2O injections all coincided with a standard curve, implying that the standard curve corresponding to the mechanism function could be determined as the most probable mechanism function under such conditions. Alternatively, the kinetic index n was not an integer, indicating that the actual reaction mechanism of JM oil shale deviated from the ideal model.

(a)

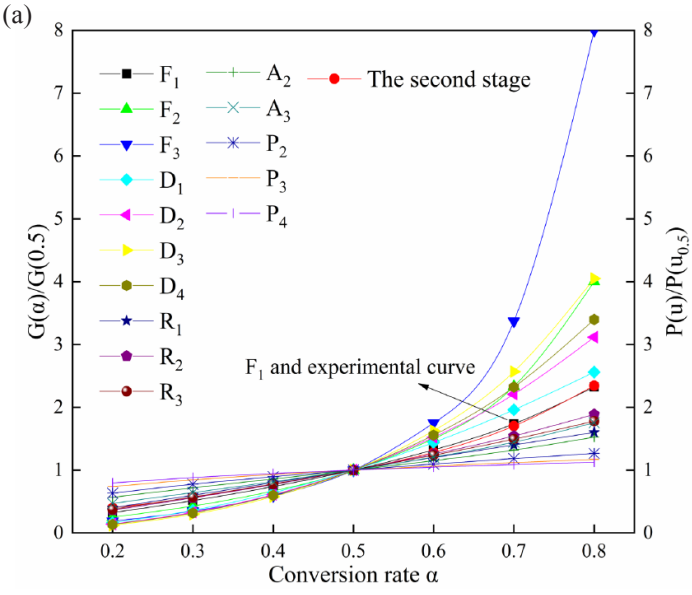
F1
F2
F3
D1
D2
D3
D4
R1
R2
R3
A2
A3
P2
P3
P4
The second stage
F1 and experimental curve
G(α)/G(0.5)
P(u)/P(u0.5)
Conversion rate α
0.2
0.3
0.4
0.5
0.6
0.7
0.8
0
1
2
3
4
5
6
7
8

(b)

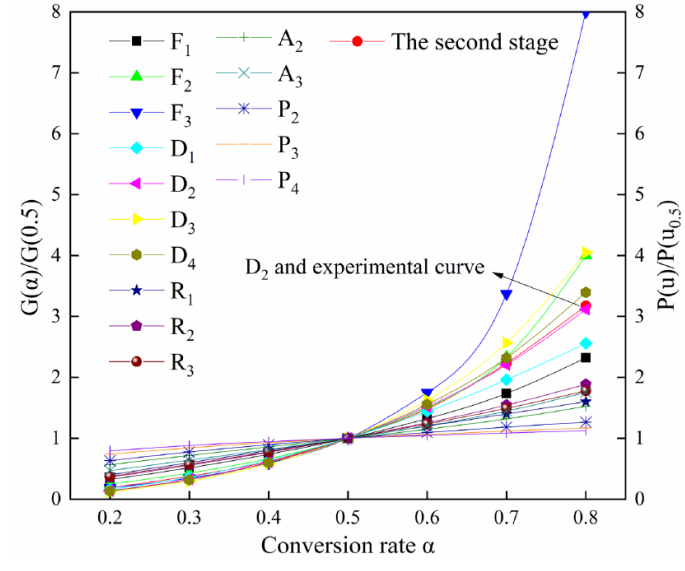
F1
F2
F3
D1
D2
D3
D4
R1
R2
R3
A2
A3
P2
P3
P4
The second stage
D2 and experimental curve
G(α)/G(0.5)
P(u)/P(u0.5)
Conversion rate α
0.2
0.3
0.4
0.5
0.6
0.7
0.8
0
1
2
3
4
5
6
7
8

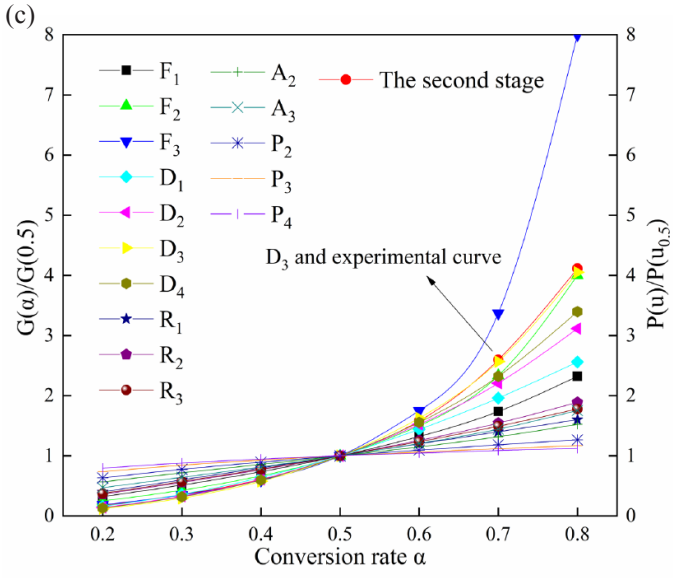

Fig. 5. Comparison of standard and experimental curves of the second stage of Jimusar oil shale pyrolysis in three different atmospheres: (a) N_2, (b) CO_2, (c) H_2O.

Figure 5 shows that the N_2 injection experimental curve tallied with the mechanism function F_1, while the CO_2 injection curve coincided with the mechanism function D_2, and that of the H_2O injection was in line with the standard curve D_3. All experimental curves coincided with the standard curve, illustrating that the kinetic exponent *n* was an integer. Table 2 presents the mechanism functions of oil shale organic matter pyrolysis in N_2, CO_2, and H_2O atmospheres as $f(\alpha) = 1-\alpha$, $f(\alpha) = [-\ln(1-\alpha)]^{-1}$, and $f(\alpha) = 1.5(1-\alpha)^{2/3}[1-(1-\alpha)^{1/3}]^{-1}$, respectively. Among these, F_1 belonged to the first-order reaction model, indicating that the total reaction rate of the reaction system after the N_2 injection under these reaction conditions was regulated by the chemical reaction process. D_n was part of the diffusion model, implying that the diffusion resistance was negligible relative to the chemical reaction rate, and that the total reaction rate was dominated by the diffusion rate under these reaction conditions. Therefore, CO_2 and H_2O injections changed the pyrolysis mechanism of organic matter in JM oil shale, by greatly enhancing this process and accelerating the chemical reaction, while the diffusion resistance could not be ignored.

After verifying the mechanism function, a series of $G(a)–EP(u)/\beta R$ relationship curves were generated at specific β, and the least squares method was used for linear fitting. The slope of the fitting line was the pre-exponential factor A. Three dynamic factors of the second stage of JM oil shale pyrolysis in different atmospheres and at different β were determined; the results are given in Table 4. The R^2 values ranged from 0.9881 to 0.9998 after fitting with a high linear correlation, highlighting the reliability of the data. The

pre-exponential factors for the second stage of JM oil shale pyrolysis after N_2, CO_2, and H_2O injections ranged from 1.113×10^{17} to 1.340×10^{17} s^{-1}, 5.161×10^{25} to 6.272×10^{25} s^{-1}, and 6.839×10^{29} to 7.800×10^{29} s^{-1} at different values of β, respectively.

Table 4. Kinetic triplets for the second stage of Jimusar oil shale pyrolysis at 10, 20, and 30 °C/min

Atmosphere	β, °C·min^{-1}	E, kcal·mol^{-1}	A, s^{-1}	$f(\alpha)$	R^2
N_2	10	56.34–63.72	1.113×10^{17}	1–α	0.9982
	20		1.198×10^{17}		0.9998
	30		1.340×10^{17}		0.9996
CO_2	10	77.47–105.11	6.272×10^{25}	$[-\ln(1-\alpha)]^{-1}$	0.9993
	20		6.018×10^{25}		0.9892
	30		5.161×10^{25}		0.9881
H_2O	10	71.84–138.35	7.800×10^{29}	$1.5(1-\alpha)^{2/3}[1-(1-\alpha)^{1/3}]^{-1}$	0.9993
	20		6.839×10^{29}		0.9968
	30		6.913×10^{29}		0.9924

Verification of the mechanism function is usually based on a comparison between the calculated results and experimental data under real reaction conditions. To verify the applicability and accuracy of the kinetic calculation method and the calculation results of the three kinetic factors, the obtained kinetic parameters E, A, and $f(\alpha)$ were used to calculate and simulate the pyrolysis process of JM oil shale, and the conversion rate curves were drawn.

The FWO method was used to validate the kinetic parameters, based on which $g(\alpha)$ was expressed using Eq. (10):

$$g(\alpha) = \frac{AE}{R\beta} e^{-5.331-1.0516\frac{E}{RT}}. \quad (10)$$

Combined with the mechanism functions $f(\alpha) = 1-\alpha$ and $g(\alpha) = -\ln(1-\alpha)$ for the second stage of JM oil shale pyrolysis after the N_2 injection, $f(\alpha) = [-\ln(1-\alpha)]^{-1}$ and $g(\alpha) = (1-\alpha)\ln(1-\alpha) + \alpha$ after the CO_2 injection, and $f(\alpha) = 1.5(1-\alpha)^{2/3}[1-(1-\alpha)^{1/3}]^{-1}$ and $g(\alpha) = [1-(1-\alpha)^{1/3}]^2$ after the H_2O injection, α was solved using Eq. (11):

$$\alpha = 1 - e^{-\frac{AE}{R\beta} e^{-5.331-1.0516\frac{E}{RT}}}. \quad (11)$$

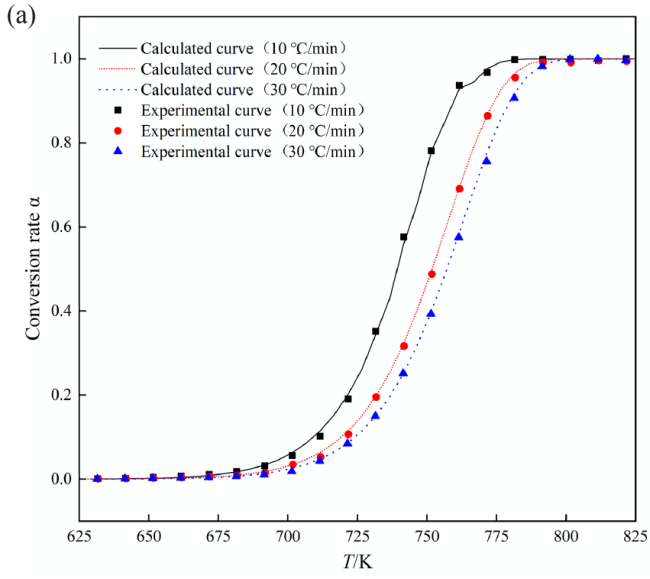
(a)
Calculated curve（10 ℃/min）
Calculated curve（20 ℃/min）
Calculated curve（30 ℃/min）
Experimental curve（10 ℃/min）
Experimental curve（20 ℃/min）
Experimental curve（30 ℃/min）
Conversion rate α
T/K

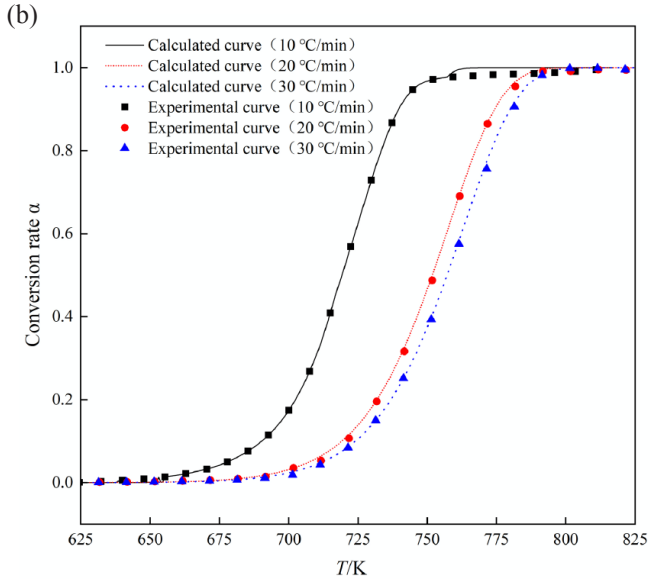
(b)
Calculated curve（10 ℃/min）
Calculated curve（20 ℃/min）
Calculated curve（30 ℃/min）
Experimental curve（10 ℃/min）
Experimental curve（20 ℃/min）
Experimental curve（30 ℃/min）
Conversion rate α
T/K

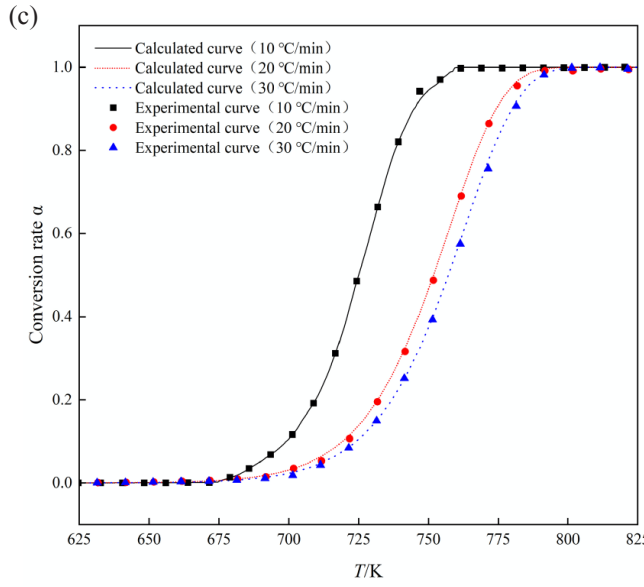

Fig. 6. Comparison of experimental and calculated α curves for Jimusar oil shale pyrolysis at different heating rates in N_2 (a), CO_2 (b), and H_2O (c) atmospheres.

The experimental temperature and actual β, E, and A measured using the FWO method were substituted into Eq. (11) to describe the change in the theoretical conversion α calculated during the second stage of JM oil shale pyrolysis at $\beta = 10$, 20, and 30 °C/min with temperature. A comparison between the theoretically calculated conversion of JM oil shale and the experimental conversion at different β values in the three atmospheres was performed. Figure 6 shows that the theoretical curves at different values of β agreed with the experimental data, indicating that the calculation method and the obtained kinetic parameters were highly accurate.

4. Conclusions

In this study, experiments on Jimusar oil shale pyrolysis with N_2, CO_2, and H_2O injections were conducted to study the influence of atmospheric differences on the oil shale pyrolysis behavior and kinetics. The following results were obtained and conclusions made.

1. Both H_2O and CO_2 injections promoted oil shale pyrolysis, increased the pyrolysis weight loss and weight loss rate of oil shale, and moved the pyrolysis zone to the low-temperature zone. Notably, the effect of H_2O was superior to that of CO_2, but both atmospheres were adversely affected by carbonate decomposition.

2. Both H_2O and CO_2 injections advanced the initial precipitation temperature of the volatiles and the peak temperatures of oil shale pyrolysis, resulting in the completion of the pyrolysis reaction in a low-temperature range and a slight widening of the half-peak width $\Delta T_{1/2}$ of the pyrolysis reaction. Additionally, both injections enhanced D, which expanded by 37.02% and 18.94%, respectively, at $\beta = 20$ °C/min. The pyrolysis reactivity of oil shale was stimulated, and H_2O was again superior to CO_2.
3. During the second stage of oil shale pyrolysis (pyrolysis of organic matter), with an increase in α, the activation energy with the N_2 injection first increased and then decreased, while with the CO_2 injection, it continuously decreased, and with the H_2O injection it fluctuated. The average activation energy of oil shale pyrolysis in both H_2O and CO_2 atmospheres was higher than that with the N_2 injection because of the secondary reaction between the oil shale volatiles and CO_2 and H_2O. The average activation energy with the H_2O injection was superior to that with the CO_2 injection.
4. During the second stage of oil shale pyrolysis (organic matter pyrolysis), the pyrolysis mechanism function was $f(\alpha) = 1–\alpha$ with the N_2 injection, $f(\alpha) = [-\ln(1–\alpha)]^{-1}$ with the CO_2 injection, and $f(\alpha) = 1.5(1–\alpha)^{2/3}[1–(1–\alpha)^{1/3}]^{-1}$ with the H_2O injection, respectively. The presence of CO_2 and H_2O alters the pyrolysis mechanism of organic matter in oil shale from a first-order model to a diffusion model.

Acknowledgements

This work was supported by the National Key Research and Development Program of China (Grant No. 2019YFA0705501), China National Postdoctoral Program for Innovative Talents (Grant No. BX2021209), and Fundamental Research Program of Shanxi Province (Grant No. 202203021222089).

The publication costs of this article were partially covered by the Estonian Academy of Sciences.

REFERENCES

1. Lu, Y., Wang, Z. J., Kang, Z. Q., Li, W., Yang, D., Zhao, Y. S. Comparative study on the pyrolysis behavior and pyrolysate characteristics of Fushun oil shale during anhydrous pyrolysis and sub/supercritical water pyrolysis. *RSC Adv*., 2022, **12**(26), 16329–16341.
2. Yang, D., Zhao, Y. S., Kang, Z. Q. Numerical simulation of in situ exploitation of oil shale by injecting high-temperature steam. *Oil Shale*, 2019, **36**(4), 483–500.
3. Zhao, J., Yang, L. S., Yang, D., Kang, Z. Q., Wang, L. Study on pore and fracture evolution characteristics of oil shale pyrolysed by high-temperature water vapour. *Oil Shale*, 2022, **39**(1), 79–95.

4. Yang, D., Wang, L., Zhao, Y. S., Kang, Z. Q. Investigating pilot test of oil shale pyrolysis and oil and gas upgrading by water vapor injection. *J. Petrol. Sci. Eng.*, 2021, **196**, 108101.
5. Bai, J. R., Hao, T. T., Yang, L., Wang, B., Wang, J. Z. Pyrolysis characteristics of oil shale in CO_2/N_2 atmosphere. *Clean Coal Technology*, 2022, **28**(7), 103–110 (in Chinese).
6. Kang, Z. Q., Wang, Z. J., Lu, Y., Cao, R., Huang, D. W., Meng, Q. R. Investigation on the effect of atmosphere on the pyrolysis behavior and oil quality of Jimusar oil shale. *Geofluids*, 2022, 1408690.
7. Wang, Q., Wang, X. M., Pan, S. Study on the structure, pyrolysis kinetics, gas release, reaction mechanism, and pathways of Fushun oil shale and kerogen in China. *Fuel Process. Technol.*, 2022, **225**, 107058.
8. Ma, Y., Li, S. Y., Wang, J., Fang, C. H. Kinetics of oil shale pyrolysis under saturated aqueous medium. *CIESC Journal*, 2010, **61**(9), 2474–2479 (in Chinese).
9. Liang, K., Liang, J., Shi, L. X., Ma, G. F., Wang, L., Wang, J., Liang, P. Effects of heating rate on the pyrolysis characteristics and kinetics of Huadian oil shale. *Journal of Mining Science and Technology*, 2018, **3**(2), 194–200 (in Chinese).
10. Zhao, S., Sun, Y. H., Lü, X. S., Li, Q. Kinetics and thermodynamics evaluation of carbon dioxide enhanced oil shale pyrolysis. *Sci. Rep.*, 2021, **11**(1), 516.
11. Kelemen, S. R., Afeworki, M., Gorbaty, M. L., Sansone, M., Kwiatek, P. J., Walters, C. C., Freund, H., Siskin, M., Bence, A. E., Curry, D. J., Solum, M., Pugmire, R. J., Vandenbroucke, M., Leblond, M., Behar, F. Direct characterization of kerogen by X-ray and solid-state ^{13}C nuclear magnetic resonance methods. *Energy Fuels*, 2007, **21**(3), 1548–1561.
12. Chen, X. P., Gu, L. F., Han, X. Q., Zhao, C. S., Liu, D. Y. Pyrolysis characteristics and ash fusion property of sludge and blended fuel of sludge and coal. *Journal of Southeast University*, 2008, **38**(6), 1038–1043 (in Chinese).
13. Qiu, P. H., Zhao, Y., Chen, X. Y., Xu, J. J., Du, Y. W., Fang, L. X., Sun, S. Z. Effects of alkali and alkaline earth metallic species on pyrolysis characteristics and kinetics of Zhundong coal. *Journal of Fuel Chemistry and Technology*, 2014, **42**(10), 1178–1189 (in Chinese).
14. Chen, J. B. *Study on Pyrolysis and Combustion Characteristics and Kinetics of Petrochemical Wastewater Sludge, Coal, and Their Blends*. PhD Thesis, Dalian University of Technology, 2016 (in Chinese).
15. Zou, S. P., Wu, Y. L., Yang, M. D., Li, C., Tong, J. M. Pyrolysis characteristics and kinetics of the marine microalgae *Dunaliella tertiolecta* using thermogravimetric analyzer. *Bioresour. Technol.*, 2010, **101**(1), 359–365.
16. Tang, L. Y., Yan, Y. X., Meng, Y., Wang, J. Y., Jiang, P., Pang, C. H., Wu, T. CO_2 gasification and pyrolysis reactivity evaluation of oil shale. *Energy Procedia*, 2019, **158**, 1694–1699.
17. Lewan, M. D., Roy, S. Role of water in hydrocarbon generation from Type-I kerogen in Mahogany oil shale of the Green River Formation. *Org. Geochem.*, 2011, **42**(1), 31–41.
18. Ceron, A. L., Konist, A. Co-pyrolysis of woody biomass and oil shale in a batch reactor in CO_2, CO_2-H_2O, and Ar atmospheres. *Energies*, 2023, **16**(7), 3145.

19. Sun, B. Z., Wang, Q., Wang, H. G., Liu, H. P., Li, S. H. Study on change of activation energy of oil shale devolatilization and combustion. *Proceedings of the CSEE*, 2011, **31**(35), 103–109 (in Chinese).
20. Wu, X. L., Lyu, L. H., Ma, Q. X., Zeng, C. Y., Zhao, T. S. Research progress of nickel-based catalysts for carbon dioxide reforming of methane. *Clean Coal Technology*, 2021, **27**(3), 129–137 (in Chinese).
21. Cui, X. J., Su, H. Y., Chen, R. X., Yu, L., Dong, J. C., Ma, C., Wang, S. H., Li, J. F., Yang, F., Xiao, J. P., Zhang, M. T., Ma, D., Deng, D. H., Zhang, D, H., Tian, Z. Q., Bao, X. H. Room-temperature electrochemical water-gas shift reaction for high purity hydrogen production. *Nat. Commun.*, 2019, **10**(1), 86.
22. Kang, Z. Q., Li, X., Yang, T., Zhao, J., Zhao, Y. S., Yang, D. Comparisons of pore structures of oil shale upon conduction and convection heating. *Chin. J. Rock Mech. Eng.*, 2018, **37**(11), 2565–2575 (in Chinese).
23. Li, S. H., Bai, J. R., Sun, B. Z., Hu, A. J., Wang, Q. Effect of heating rate on the pyrolysis characteristics of oil shales. *Chemical Engineering*, 2007, **215**(1), 64–67 (in Chinese).
24. Duan, W. J., Yu, Q. B., Xie, H. Q., Qin, Q. Pyrolysis of coal by solid heat carrier – experimental study and kinetic modeling. *Energy*, 2017, **135**, 317–326.
25. Chi, H. Y., Li, H. J., Xu, K., Liu, H., Su, S., Hu, S., Xiang, J. Comprehensive study on the effect of CO_2 on coal pyrolysis at fast heating rate. *Energy Rep.,* 2021, **7**(7), 1369–1378.
26. Bai, J. R., Pan, S. H., Wang, Q., Chi, M. S., Li, T. Pyrolysis characteristics of Inner Mongolia oil shales with different organic matter contents. *Chemical Industry and Engineering Progress*, 2017, **36**(7), 2428–2435 (in Chinese).
27. Li, H. W., Wang, X. H., Li, X., Su, Y., Zhang, S. C., Song, Q. S., Tang, Z. F. Experimental studies on *n*-heptane pyrolytic characteristics in CO_2/H_2O atmosphere. *J. Anal. Appl. Pyrolysis*, 2021, **154**, 104999.
28. Policella, M., Wang, Z. W., Burra, K. G., Gupta, A. K. Characteristics of syngas from pyrolysis and CO_2-assisted gasification of waste tires. *Applied Energy*, 2019, **254**, 113678.
29. Du, J. X., Yu, J., Qiao, L., Reina, T. R., Sun, L. H. The reaction mechanism and sulfur evolution during vulcanized nature rubber pyrolysis in the atmosphere of H_2O: A ReaxFF molecular dynamics study. *Polym. Degrad. Stabil.*, 2022, **203**, 110064.
30. Aljaziri, J., Gautam, R., Alturkistani, S., Fiene, G. M., Tester, M., Sarathy, S. M. On the effects of CO_2 atmosphere in the pyrolysis of *Salicornia bigelovii*. *Bioresour. Technol. Rep.*, 2022, **17**, 100950.
31. Kim, S., Yang, W. Y., Lee, H. S., Tsang, Y. F., Lee, J. H. Effectiveness of CO_2-mediated pyrolysis for the treatment of biodegradable plastics: A case study of polybutylene adipate terephthalate/polylactic acid mulch film. *J. Clean. Prod.*, 2022, **372**, 133763.
32. Chen, C. X., Lu, Z. G., Ma, X. Q., Long, J., Peng, Y. N., Hu, L. K., Lu, Q. Oxy-fuel combustion characteristics and kinetics of microalgae *Chlorella vulgaris* by thermogravimetric analysis. *Bioresour. Technol.*, 2013, **144**, 563–571.